International Conference on Renewable Energies and Power Quality (ICREPQ'18)
Salamanca (Spain), 21th to 23th March, 2018
Renewable Energy and Power Quality Journal (RE&PQJ)
ISSN 2172-038 X, No.16 April 2018

Comparative study of torque ripple minimization techniques for a three-phase switched reluctance motor

de Paula, M. V.[1], Barros, T. A. S.[1], Santos Neto, P. J. [1], de Souza, R. R. [1], and Ruppert Filho, E. [1]

[1] Faculty of Electrical and Computer Engineering, University of Campinas
Campus of Campinas – Campinas (Brazil)
Phone number: +55 19 3521-8961, e-mail: **mvpaula@outlook.com**

Abstract. Switched reluctance machines (SRM) raise advantages such as ruggedness, simplicity and fault tolerance, which highlights these machines among other topologies for variable speed applications. However, inherent drawbacks as high torque ripple and acoustic noise occur, both caused by the doubly salient structure and drive principle. This paper presents an investigation regarding SRMs torque ripple mitigation. The principles of SRM are addressed to explain the torque ripple presence. Then, instantaneous torque control (ITC) techniques, such as common torque sharing functions (TSF), direct instantaneous torque control (DITC) and direct torque control (DTC) are discussed and compared. Simulations are performed to verify the control algorithms. The simulated system consists of a control block containing the control algorithm of one aforementioned technique, an asymmetric half bridge (AHB), an 80 V power supply, and an 1,5 kW, 12/8 SRM. Simulations convey that, among the TSFs, the sinusoidal TSF arise lower torque ripple. After that, the sinusoidal TSF was compared to the other methods, in this case, sinusoidal TSF produced minor torque ripple from 0 to 1000 rpm and for higher speeds, DITC presented smaller torque ripple. It is possible to conclude that TSF is recommended for low speed applications, while DITC is suggested for higher speed applications.

Key words

Switched Reluctance Motor, Torque Ripple Reduction, Direct Torque Control, Direct Instantaneous Torque Control, Torque Sharing Function, Instantaneous Torque Control.

1. Introduction

Ruggedness, simplicity of design, fault tolerance, wide speed range and high temperature operation make switched reluctance motors (SRM) an attractive solution for many applications, especially those that require variable speed operation [1], [2]. Torque ripple is an effect seen in machines referring to a periodic fluctuation in output torque as the motor shaft rotates. Plenty of applications require highly smooth torque, e.g. precision tools, robotics, electric vehicles, and aeronautics [3], [4]. For this reason, torque ripple reduction has been a recurrent object of study and many techniques have been proposed [3]-[13].

Torque ripple can be minimized by either mechanical methods or electronic control techniques [13], [14]. The mechanical methods consist of changing the machine structure in order to manipulate the magnetic flux. Thus, smaller reluctance variation is produced during each stroke, leading to smaller torque ripple. Controversially, these structural changes limit the operating range of the machine. Moreover, electronic control algorithms can diminish the electromagnetic torque fluctuations by controlling sets of parameters, for instance, reference electric current, turn-on and turn-off angles, and supply voltage [13]. These parameters can be controlled directly or indirectly.

This paper focus on the investigation control techniques that minimize torque ripple. Initially, the SRM torque ripple production must be understood, hence section 2 shows the SRM electrodynamics and drive principle. After that, commonly used torque ripple minimization techniques are presented in section 3. In section 4, simulation results are revealed and compared. The comparison implies that among the torque sharing functions (TSFs), the sinusoidal TSF has smaller torque ripple. When compared to direct torque control (DTC) and direct instantaneous torque control (DITC), the sinusoidal TSF is recommended for reduced speeds and idle, whilst between 1000 rpm up to 2100 rpm, DITC overcome the other techniques. Beyond this point, none of the methods is capable of regulating torque and the speed and torque regulation is performed by current chopping control (CCC) in single pulse mode.

2. SRM Torque Production and Drive Principles

SRMs are composed by a doubly salient structure, where only stator poles have windings (Fig. 1(a)). When these windings are energized, the closest rotor pole is attracted, chasing the alignment between stator and rotor poles. This process changes the rotor position, implying in inductance variation according to the rotor angular position [10].

Fig. 1(b) shows the ideal inductance profile for a SRM, where θ_{un} and θ_{al} stand for the start of the unaligned and aligned regions respectively. Note that torque direction strictly depends on the derivative of inductance $(dL(\theta)/d\theta)$. When phase current is applied during positive inductance derivative, positive torque is produced. If the phase energization occur during negative derivative of the inductance, then, negative torque is produced as depicted in Fig. 1(b).

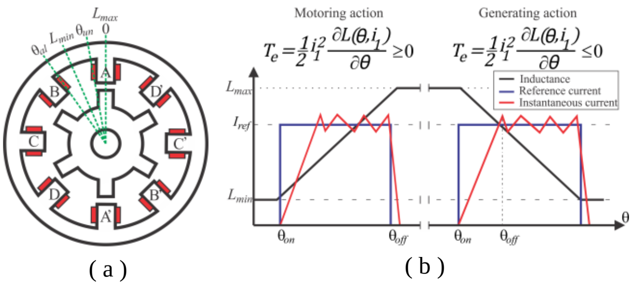

Fig. 1. a) MRV structure; b) Inductance profile and MRV torque production in motoring and generating modes.

Through the coenergy analysis, assuming magnetic decoupling among the phases, (1) rises, where T_k is the phase torque, $\partial W'/\partial\theta\,|_{i_k}$ is the partial derivative of coenergy with respect to the rotor angle θ with a fixed electric phase current i_k, and $\lambda_k(i,\theta)$ is the electric current and rotor position dependent flux linkage. If magnetic linearity is also considered, the flux linkage becomes: $\lambda_k = L(\theta)i_k$, and (1) can be rewritten as (2), where $dL(\theta)/d\theta$ is the derivative of inductance with respect to rotor angular position. The total torque produced is given by the sum of each phase torque.

$$T_k = \left.\frac{\partial W'}{\partial \theta}\right|_{i_k} = \frac{d}{d\theta}\int_0^{i_k} \lambda_k(i,\theta)di \qquad (1)$$

$$T_k = \frac{i_k^2}{2}\frac{dL(\theta)}{d\theta} \qquad (2)$$

As aforementioned, inspecting (2), one perceive that torque production hinges on the slope of inductance profile. Moreover, (2) also implies that torque is independent of the electric current signal because of their quadratic relation.

Torque ripple (T_{ripple}) can be estimated as the difference between maximum and minimum instantaneous torque (T_{inst}) in one electrical period divided by the average torque $(\bar{T})$ in the same period as shown in (3).

$$T_{ripple} = \frac{\max(T_{inst}) - \min(T_{inst})}{\bar{T}} \qquad (3)$$

For continuous operation, the SRM must be driven by a power electronic converter. Usually, an asymmetric half bridge (AHB) converter is used. The AHB is composed by two power switches and two diodes per phase. This topology can be employed for any number of motor phases. Moreover, AHB enables four-quadrant operation, which is a requirement for many applications, such as electric vehicles propulsion systems [2]. Fig. 2(a) shows an AHB for the three phases SRM used in this study. Three voltage levels can be applied to the phase according to the switch states as shown in Fig. 2. If two switches are turned on, positive state is applied to SRM phase (Fig. 2(b)), if both switches are turned off, phase terminals will experience negative voltage (Fig. 2(c)), this state is known as demagnetization, lastly, if only one switch is enabled, zero voltage will be on the SRM phase, characterizing the freewheeling state (Fig. 2(d)).

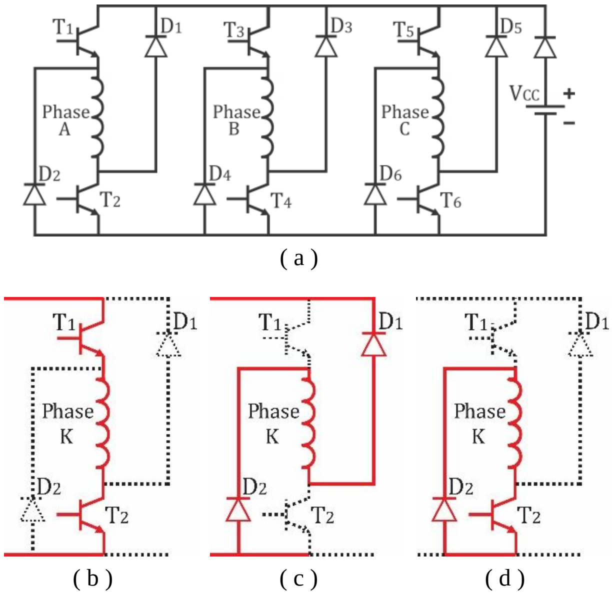

Fig. 2. a) AHB for three -phase SRM; b) Positive state or magnetization; c) Negative state or demagnetization; d) Zero state or freewheeling.

3. Torque Ripple Minimization Techniques

Electronic torque ripple minimization techniques are based on optimizing the control parameters as turn-on and turn-off angles, the supply voltage and the electric current level. This paper focus on techniques that control the instantaneous torque, named instantaneous torque control (ITC).

In ITC, the reference current or voltage is calculated in real time based on the torque reference and rotor angular position. Besides that, the torque/speed plan cannot be entirely covered because above certain speeds, the current regulation is not possible. On the other hand, torque ripple can be minimized by regulating the control parameters.

Following subsections explain some ITC methods that are studied in this work.

A. Torque Sharing Function

One can control the torque indirectly by controlling the electric current. This technique is called current profiling technique (CPT) and consists in force the current to follow a reference profile. This reference can be generated online [3], [13] or offline [8].

Considering that the electric current can be properly controlled, then the torque production can be shared between the phases in such a way that the sum of electromagnetic torque produced by the phases is equal to the torque reference. Methods that use this principle are referred as TSFs. In such cases, the total reference torque (T^*) is divided among the phases, generating a reference torque for each phase k (T_k^*). This division depends on the rotor angular position (θ) and must follow a profile defined as,

$$T_k^*(\theta) = \begin{cases} 0 & ,0 \le \theta \le \theta_{on} \\ T^* f_{rise}(\theta) & ,\theta_{on} \le \theta \le \theta_{on} + \theta_{ov} \\ T^* & ,\theta_{on} + \theta_{ov} \le \theta \le \theta_{off} + \theta_{ov} \\ T^* f_{fall}(\theta) & ,\theta_{off} + \theta_{ov} \le \theta \le \theta_{off} \\ 0 & ,\theta_{off} \le \theta \le \theta_{al} \end{cases} \quad (3)$$

where θ_{on}, θ_{off}, θ_{ov}, and θ_{al} are the turn-on, the turn-off, the overlapping, and the alignment angles respectively. $f_{rise}(\theta)$ and $f_{fall}(\theta)$ are the rotor angular position dependent functions that takes the reference from 0 to T^* and vice-versa respectively. In the literature, it is possible to find many forms for these functions, such as linear, sinusoidal, exponential, cubic or piecewise form [3], [6], [7], [9], [10]. After being generated, the reference torque is turned into a reference current through a look-up table or through an equation.

In this study, linear, sinusoidal, exponential and cubic TSFs are implemented and compared regarding torque ripple production throughout the operating speed range. The choice of the angles has high influence over the torque ripple production. Hence, the angles must be such that during commutation, the sum of the torques produced by the phases is always equal to the total reference torque.

The rise and fall equation for linear, sinusoidal, exponential and cubic TSFs are given by equations (4) to (7), where the indexes lin, sin, exp and cub refer to the linear, sinusoidal, exponential and cubic TSFs, respectively.

$$Linear \begin{cases} f_{rise}^{lin}(\theta) = \dfrac{1}{\theta_{ov}}(\theta - \theta_{on}) \\ f_{fall}^{lin}(\theta) = 1 - \dfrac{1}{\theta_{ov}}(\theta - \theta_{off}) \end{cases} \quad (4)$$

$$Sinusoidal \begin{cases} f_{rise}^{\sin}(\theta) = \dfrac{1}{2} - \dfrac{1}{2}\cos\dfrac{\pi}{\theta_{ov}}(\theta - \theta_{on}) \\ f_{fall}^{\sin}(\theta) = \dfrac{1}{2} + \dfrac{1}{2}\cos\dfrac{\pi}{\theta_{ov}}(\theta - \theta_{off}) \end{cases} \quad (5)$$

$$Exponential \begin{cases} f_{rise}^{\exp}(\theta) = 1 - \exp\left(\dfrac{-(\theta - \theta_{on})^2}{\theta_{ov}}\right) \\ f_{fall}^{\exp}(\theta) = \exp\left(\dfrac{-(\theta - \theta_{off})^2}{\theta_{ov}}\right) \end{cases} \quad (6)$$

$$Cubic \begin{cases} f_{rise}^{cub}(\theta) = \dfrac{3}{\theta_{ov}^2}(\theta - \theta_{on})^2 - \dfrac{2}{\theta_{ov}^3}(\theta - \theta_{on})^3 \\ f_{fall}^{cub}(\theta) = 1 - f_{rise}^{cub}(\theta - \theta_{off} + \theta_{on}) \end{cases} \quad (7)$$

Fig. 3 presents the torque profile generated by each of these TSFs.

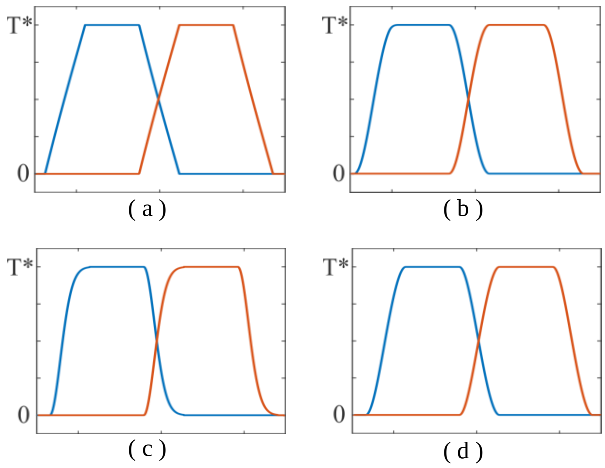

Fig. 3. TSFs profiles: a) Linear; b) Sinusoidal; c) Exponential; d) Cubic.

B. Direct Torque Control

Direct torque control (DTC) is a well-known control method for induction machines. DTC can be adapted to fit SRM requirements [16], [17]. The basic principle of this method is to maintain the stator flux linkage and the instantaneous torque within hysteresis bands by applying the different states shown in Fig. 2. The states have the capability of changing the orientation of the flux linkage vector as well as the amplitude. Changes in flux vector are connected to the torque production, thus, the torque can be controlled. This process of increasing or decreasing the flux linkage to control the electromagnetic torque is named flux acceleration and deceleration, respectively [18].

The choice of voltage state depends on the rotor angular position θ, the flux linkage error and the instantaneous torque error. Fig. 4 depicts the state vectors to be applied according to rotor position. The vector space is divided in six sectors (S_0-S_5).

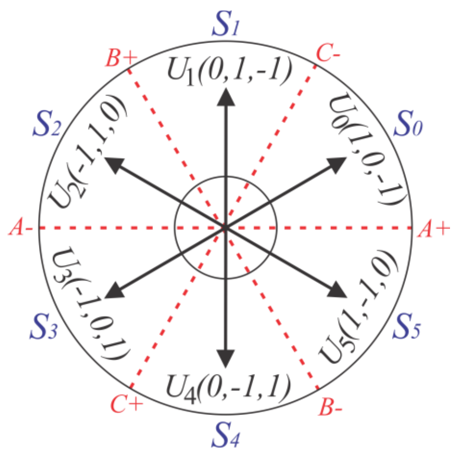

Fig. 4. State vectors according to rotor angular position.

The instantaneous flux linkage module and the rotor angle position are found through Clarke transformation. Alpha and beta components are calculated as

$$\begin{cases} \lambda_\alpha = \lambda_a - \lambda_b \cos 60^o + \lambda_c \cos 60^o \\ \lambda_\beta = \lambda_b \sin 60^o - \lambda_c \sin 60^o \end{cases} \quad (8)$$

where λ_α and λ_β are respectively the α-axis and β-axis portion of the flux linkage, and λ_a, λ_b and λ_c are respectively the A, B and C phases flux linkage.

The total flux linkage λ_{tot} is given by:

$$\lambda_{tot} = \sqrt{\lambda_\alpha + \lambda_\beta} \quad (9)$$

and the rotor position can be estimated through

$$\theta = \arctan 2 \frac{\lambda_\beta}{\lambda_\alpha} \quad (10)$$

where $arctan2(x)$ is the four quadrant arctangent pertaining to the interval $-\pi \leq arctan2(x) \leq \pi$.

Table I summarizes the voltage state choice, where positive, negative and freewheeling states are represented as 1, -1, and 0, respectively. For instance, if $60 \leq \theta \leq 120^o$ and both torque and flux linkage reach the upper band of the hysteresis, the vector U_5 should be applied. Then, the states 1, -1 and 0 must be applied to phases A, B and C, respectively.

Table I. - DTC switching table for three-phase SRM.

	Relationship			
Angular position (θ)	$\lambda \uparrow$ $T \uparrow$	$\lambda \uparrow$ $T \downarrow$	$\lambda \downarrow$ $T \uparrow$	$\lambda \downarrow$ $T \downarrow$
$0 - 60^o$	$0,1,-1$	$1,-1,0$	$-1,1,0$	$0,-1,1$
$60 - 120^o$	$-1,1,0$	$1,0,-1$	$-1,0,1$	$1,-1,0$
$120 - 180^o$	$-1,0,1$	$0,1,-1$	$0,-1,1$	$1,0,-1$
$180 - 240^o$	$0,-1,1$	$-1,1,0$	$1,-1,0$	$0,1,-1$
$240 - 300^o$	$1,-1,0$	$-1,0,1$	$1,0,-1$	$-1,1,0$
$300 - 360^o$	$1,0,-1$	$0,-1,1$	$0,1,-1$	$-1,0,1$

C. Direct Instantaneous Torque Control

Introduced by Inderka [14], direct instantaneous torque control (DITC) is a closed loop control technique that employs double band hysteresis to control torque directly. The method dynamically shares the torque amongst the phases during phase commutation. However, instead of using predetermined function, as in the TSF methods, the control algorithm applies different switching states according to the enable signal and torque from the phases. While the back electromagnetic force is equal or lesser than the DC-bus voltage, DITC can be efficiently performed.

The phases are considered enabled while in the dwell interval ($\theta_{on} \leq \theta \leq \theta_{off}$). During commutation, there are two switching logics applied, one for incoming phases and one for outgoing phases. The state machines for each case are depicted in Fig. 5, where T_e is the torque error, $thlm$ is the medium low threshold, $thhm$ is the medium high threshold, thh is the highest threshold and thl is the lowest threshold. The switching logic for single conduction and for the outgoing phase during commutation is the same logic used in soft chopping (Fig. 5(a)). On the other hand, for the incoming phase during commutation, the switching logic allow the demagnetization state with the condition that the states never change from 1 to -1 directly or vice versa, that condition avoids hard chopping and ensure smoother torque (Fig. 5(b)).

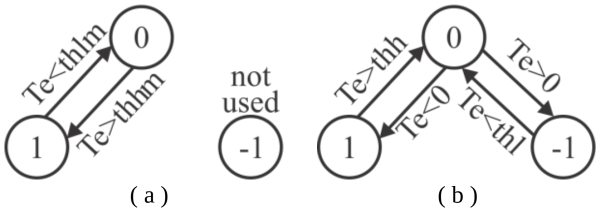

Fig. 5. State machines for DITC hysteresis; a) Single conduction and outgoing phase during commutation; b) Incoming phase during commutation.

Table II summarizes the switching rules for reaching adequate torque commutation amongst phases in DITC [9], [21], [22]. During commutation, if the incoming phase is not able to achieve the required torque, then, the outgoing phase is controlled to aid the torque production, otherwise, if the incoming phase is capable of regulating the torque, the outgoing phase is demagnetized. When the turn-off angle is achieved, demagnetization is also applied to the phase.

Table II. - Commutation strategy table of three-phase SRM for DITC

Phase enable			Phase state		
$k-1$	k	$k+1$	$k-1$	k	$k+1$
0	0	0	x	x	x
1	0	0	1/0	x	x
1	1	0	1/0/-1	1/0	x
0	1	0	-1/x	1/0	x
0	1	1	x	1/0/-1	1/0
0	0	1	x	-1/x	1/0

The switching rules presented in Table II are responsible for applying three conditions, which ensure low torque oscillations:

1) Avoid hard-chopping to minimize switching losses and reduce torque ripple;
2) Prioritize the incoming phase for torque production;
3) Maintain the outgoing phase in freewheeling state for as long as possible.

4. Simulation Results

To verify the methods, a MATLAB/Simulink model with the aforementioned techniques was built based on a 3-phase, 12/8, 1,5 kW at the base speed of 1500 rpm. The model was generated through experimentally acquired magnetization characteristics [21]. The supply voltage was fixed at 80 V. The control system block diagram in Fig. 6 summarizes the control strategy used for the simulations. The speed error passes through a PI controller to generate the torque reference. Then, the torque control algorithm of the current technique judges the conditions according to rotor angular position, electric current and voltage. The judgement passes through a switching logic block to generate the gate signal and drive the SRM.

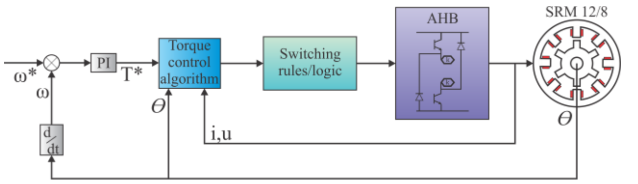

Fig. 6. Control system block diagram for instantaneous torque control techniques studied.

The simulations were performed from 100 rpm up to the point where the speed could not be tracked (1300 rpm for DTC and 2100 rpm for DITC and TSF) in steps of 200 rpm to cover the entire speed range. After the simulations, torque ripple was calculated through (3) for every aforementioned method in each speed.

A. Conventional TSFs Comparison

Linear, sinusoidal, cubic and exponential TSFs were implemented and compared regarding torque ripple through the entire speed range with the load torque fixed at 2 N.m. The angles used for the TSFs generation are the same for all the TSFs: $\theta_{on} = 24^o$, $\theta_{ov} = 6^o$ and $\theta_{off} = 39^o$. The results are presented in Fig. 7. One can see that, for the studied SRM, the linear, the sinusoidal and the cubic TSFs arise similar torque ripple with maximum divergence of 10,53% at 1700 rpm. However, the sinusoidal TSF has: 1) simpler formulation, facilitating the implementation, and 2) slightly better results bellow the base speed. Also, the exponential TSF generate the highest torque ripple beginning at 700 rpm. Hence, the sinusoidal TSF is chosen to be further compared to the other implemented methods.

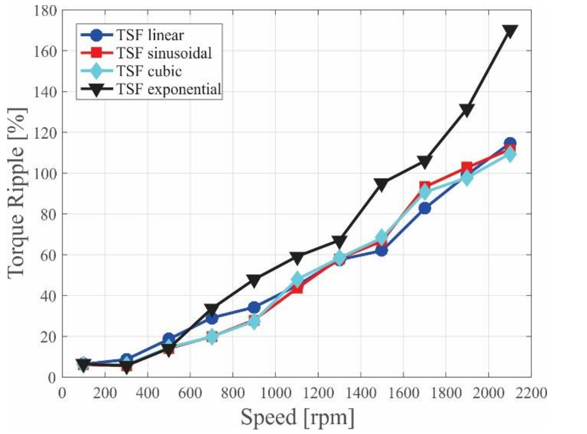

Fig. 7. Comparison of different TSFs regarding torque ripple through speed range.

B. TSF, DTC and DITC Comparison

Fig. 8 outline the instantaneous torque produced by the SRM using sinusoidal TSF, DTC and DITC at a low speed (200 rpm) and at a medium speed (600 rpm). The reference torque is accurately followed and the speed tracking capability is also achieved. In addition, speed and torque detailed waveforms are depicted for each simulated method in 200 rpm and 600 rpm. The waveforms show that with DITC the number of switches per period are reduced when compared to TSF and DTC, leading to smaller switching losses.

After the simulations, torque ripple for each speed was calculated through (3) and stored. The results are exposed in Fig. 9. As can be seen, from 100 rpm up to 950 rpm, the sinusoidal TSF presents lower torque ripple. Above 950 rpm speed DITC exhibit smaller electromagnetic torque oscillation. DTC exhibit good behavior from 100 rpm to

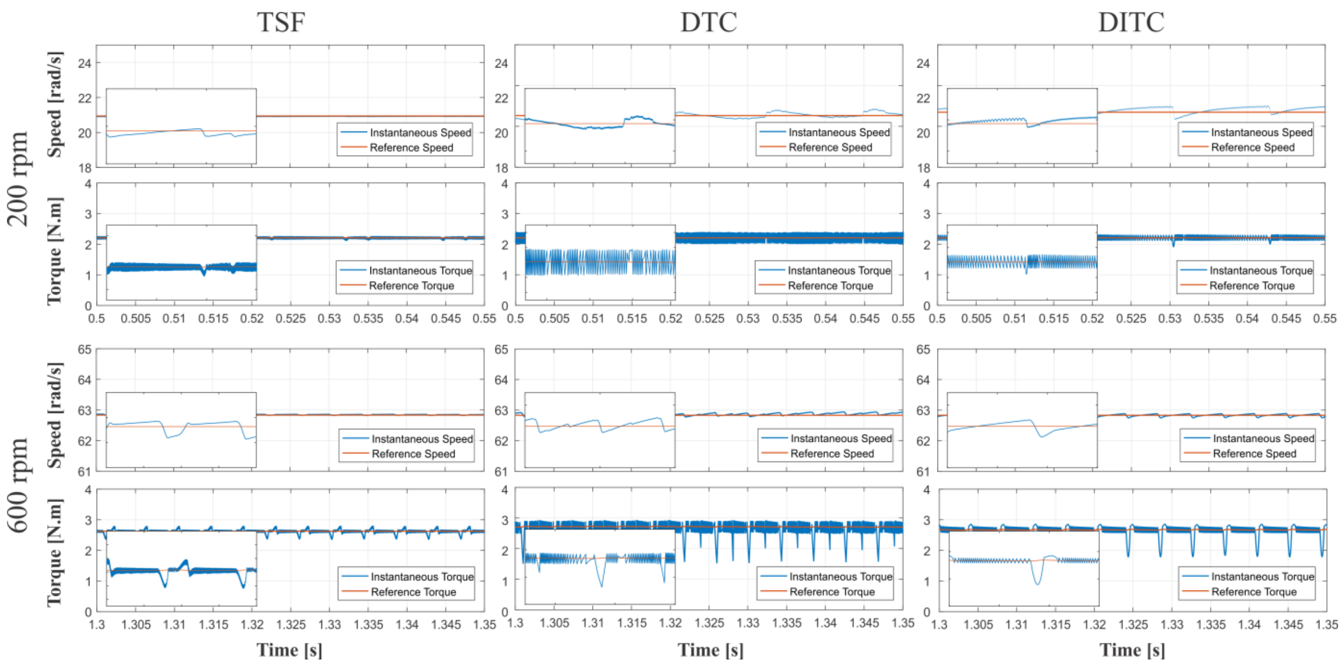

Fig. 8. Speed tracking capability and instantaneous torque produced at 200 rpm and 600 rpm for sinusoidal TSF, DITC and DITC.

300 rpm with the torque ripple bellow 20%, on the other hand, the torque ripple values escalate with speed increase.

The maximum speed achieved with DTC is 1300 rpm, while with DITC and TSF 2100 rpm can be achieve without losing the speed regulation ability.

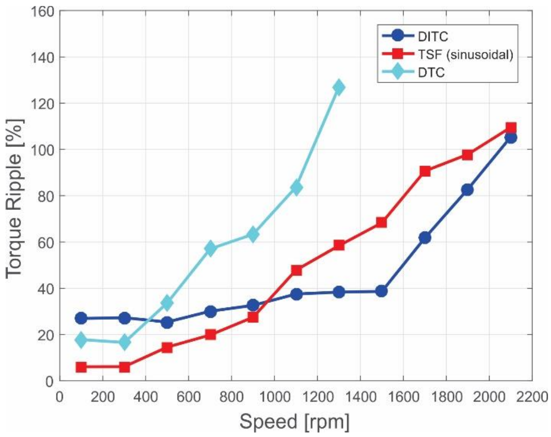

Fig. 9. Comparison of DITC, sinusoidal TSF and DTC regarding torque ripple in through speed range.

5. Conclusion

This paper investigated different electronic control torque ripple mitigation techniques, where the instantaneous torque is regulated indirectly in all techniques and the speed is controlled in the outer loop by a PI controller. The basic principles of SRM and of the control techniques were presented and simulations were performed to verify the methods. Initially, four types of TSF were compared and sinusoidal TSF demonstrated the smallest torque ripple. Afterwards, the sinusoidal TSF, DTC and DITC results were compared. Considering the SRM studied, sinusoidal TSF presented smaller torque ripple and is recommended for low speed applications (up to 1000 rpm), although, for high speed applications (from 1000 rpm up to 2100 rpm), DITC surpassed the sinusoidal TSF in terms of torque oscillation.

References

[1] M. Krishnamurthy, C. S. Edrington, A. Emadi, P. Asadi, M. Ehsani, and B. Fahimi, "Making the case for applications of switched reluctance motor technology in automotive products," IEEE Transactions on Power Electronics, vol. 21, no. 3, pp. 659–675, May 2006.

[2] Gan, J. Wu, S. Yang, and Y. Hu, "Phase current reconstruction of switched reluctance motors from dc-link current under double high-frequency pulses injection," IEEE Transactions on Industrial Electronics, vol. 62, no. 5, pp. 3265–3276, May 2015.

[3] R. Mikail, Y. Sozer, I. Husain, M. Islam, and T. Sebastian, "Torque ripple minimization of switched reluctance machines through current profiling," in 2011 IEEE Energy Conversion Congress and Exposition, Sept 2011, pp. 3568–3574.

[4] R. Mikail, I. Husain, M. S. Islam, Y. Sozer, and T. Sebastian, "Four quadrant torque ripple minimization of switched reluctance machine through current profiling with mitigation of rotor eccentricity problem and sensor errors," IEEE Transactions on Industry Applications, vol. 51, no. 3, pp. 2097–2104, May 2015.

[5] Y. Guo, Q. Ma, and W. Ye, "Comparative study on torque ripple suppression method of three-phase 6/4 switched reluctance motor," in 2016 IEEE International Conference on Aircraft Utility Systems (AUS), Oct 2016, pp. 356–361.

[6] Ye, B. Bilgin, and A. Emadi, "An extended-speed low-ripple torque control of switched reluctance motor drives," IEEE Transactions on Power Electronics, vol. 30, no. 3, pp. 1457–1470, March 2015.

[7] ——, "An offline torque sharing function for torque ripple reduction in switched reluctance motor drives," IEEE Transactions on Energy Conversion, vol. 30, no. 2, pp. 726–735, June 2015.

[8] V. Petrus, A. C. Pop, C. S. Martis, V. Iancu, and J. Gyselinck, "Direct instantaneous torque control of srms versus current profiling - comparison regarding torque ripple and copper losses," in 2012 13th International Conference on Optimization of Electrical and Electronic Equipment (OPTIM), May 2012, pp. 366–372.

[9] V. P. Vujicic, "Minimization of torque ripple and copper losses in switched reluctance drive," IEEE Transactions on Power Electronics, vol. 27, no. 1, pp. 388–399, Jan 2012.

[10] X. D. Xue, K. W. E. Cheng, and S. L. Ho, "Optimization and evaluation of torque-sharing functions for torque ripple minimization in switched reluctance motor drives," IEEE Transactions on Power Electronics, vol. 24, no. 9, pp. 2076–2090, Sept 2009.

[11] K. Russa, I. Husain, and M. E. Elbuluk, "Torque-ripple minimization in switched reluctance machines over a wide speed range," IEEE Transactions on Industry Applications, vol. 34, no. 5, pp. 1105–1112, Sept 1998.

[12] S. Kurian and N. G. K., "Torque ripple minimization of srm using torque sharing function and hysteresis current controller," in 2015 International Conference on Control Communication Computing India (ICCC), Nov 2015, pp. 149–154.

[13] Husain, "Minimization of torque ripple in srm drives," IEEE Transactions on Industrial Electronics, vol. 49, no. 1, pp. 28–39, Feb 2002.

[14] R. B. Inderka and R. W. A. A. D. Doncker, "Ditc-direct instantaneous torque control of switched reluctance drives," IEEE Transactions on Industry Applications, vol. 39, no. 4, pp. 1046–1051, July 2003.

[15] Y. Sozer, I. Husain, and D. A. Torrey, "Guidance in selecting advanced control techniques for switched reluctance machine drives in emerging applications," IEEE Transactions on Industry Applications, vol. 51, no. 6, pp. 4505–4514, Nov 2015.

[16] X. Zhao, A. Xu and W. Zhang, "Research on DTC system with variable flux for switched reluctance motor," in CES Transactions on Electrical Machines and Systems, vol. 1, no. 2, pp. 199-206, 2017.

[17] Guiying Song, Zhida Li, Zhenghan Zhao and Xiang Wang, "Direct torque control of switched reluctance motors," 2008 International Conference on Electrical Machines and Systems, Wuhan, 2008, pp. 3389-3392.

[18] A. D. Cheok and Y. Fukuda, "A new torque and flux control method for switched reluctance motor drives," in IEEE Transactions on Power Electronics, vol. 17, no. 4, pp. 543-557, Jul 2002.

[19] N. H. Fuengwarodsakul, M. Menne, R. B. Inderka, and R. W. D. Doncker, "High-dynamic four-quadrant switched reluctance drive based on ditc," IEEE Transactions on Industry Applications, vol. 41, no. 5, pp. 1232–1242, Sept 2005.

[20] H. Zeng, H. Chen, and J. Shi, "Direct instantaneous torque control with wide operating range for switched reluctance motors," IET Electric Power Applications, vol. 9, no. 9, pp. 578–585, 2015.

[21] T. A. S. Barros, P. S. Nascimento Fo, A. B. Moreira, V. S. C. Teixeira, M. G. Villalva, and E. Ruppert, "Sistema automático de caracterização de maquinas de relutância variável e modelagem não linear por interpolação utilizando smoothing splines. " Eletrônica de Potência, vol. 20, pp. 140-150, 2015.